Model of Ferromagnetic Steels for Lightning Transient Analysis

*Hongcai Chen, Yaping Du**

Department of Building Services Engineering, Hong Kong Polytechnic University, Hung Hom, Kowloon, Hong Kong
Email: ya-ping.du@polyu.edu.hk

Abstract: This paper investigates the model of structural steels used in the lightning current analysis. These ferromagnetic steels can be found in grounded structures, such as towers and buildings. An equivalent electrical circuit is presented first. Circuit parameters of these steel wires are determined numerically with an equivalent circuit approach. A rational function approximation is incorporated for developing an extended circuit model of frequency-dependent circuits used in time-domain simulations. Experiments are carried out to disclose the transient response of both steel bars and rods when they carry a surge current directly. It is found that these steel wires exhibit weak ferromagnetism, and can be represented with linear magnetic materials. The proposed modelling procedure is applied to analyse surge current sharing in a 3D steel wire/power cable system adopted in radio base stations. Good agreements with the experimental results are observed.

1. Introduction

Structural steels are the essential components of large grounded structures, such as buildings [1-3], towers [4, 5] and others [6]. These components are not the part of the electrical equipment, but conduct surge currents when exposed to lightning discharges or other unpredictable transients. In these situations, structural steels should be taken into consideration, for example, in the analysis of lightning current sharing among the cables bonded to a steel structure. Unfortunately, experimental data of structural steels is not available in the literature, and transient models have not been well addressed either. One possible solution is to represent the steels with non-ferromagnetic or perfect conductors [7]. Such an approach could lead to a significant error as magnetic properties of the structural steels are not considered.

Characteristics of electrical steels [8, 9], such as those used in transformers and motors have been well addressed. However, such data could not be used directly for structural steels in the lightning transient analysis. Firstly, characteristic curves of electrical steels are obtained by injecting a current into coils mounted on the steel examples. While the structural components carry the lightning current directly, and could experience the magnetic field much more significant than the electrical steels. Secondly, existing test instruments (e.g., vector network analyzer) are not capable of providing a high-amplitude testing current.

Many numerical computation methods are available for analyzing electromagnetic phenomena associated with wire structures. The Partial Element Equivalent Circuit (PEEC) method [10-16] is one great alternative to solving lightning currents in the wire system [10, 17]. It transforms an electromagnetic (EM) problem into a system of equivalent circuits. EM couplings of wires could be easily converted into equivalent circuits. PEEC models of 3D non-magnetic conductors with eddy current present have been addressed in [17-19]. Extended PEEC formulations for analyzing magnetic plates have been developed as well [20-24]. The effects of eddy current in thin magnetic plates has been discussed using an analytical formula [21]. PEEC modelling of magnetic wires for lightning current analysis, however, has not been addressed in the literature.

In this paper, we present the model of structural steels for transient analysis under the 1st lightning return stroke current or the current with similar frequency spectrum. Firstly, the equivalent model of steel wires is presented using the concept of external inductance and internal impedance of individual wires. An equivalent circuit approach is provided for modelling eddy current in steel wires with arbitrary cross section, and subsequently evaluating wire impedance. Secondly, a rational function approximation technique [25-27] is applied to obtain equivalent frequency-independent parameters of frequency-dependent circuits for time-domain simulations. An experimental study on the surge response of structural steels is presented, and the nonlinear material property of the steels under the impulse current is addressed. Based on the proposed model, a simulation tool TAES [5] is applied to analyze surge current sharing in a 3D wire system consisting of power cables and steel bars. The results of experimental validation are presented finally in the paper.

2. Circuit Model of Steel Wires

The 1st lightning return stroke current [28] has a representative waveform of 10/350 μs. Its primary frequency is in the range of several tens kHz. In this frequency range, electric field coupling among a group of closely-spaced conductors and cables is negligible. Modelling of mutual capacitances then is not addressed in this paper. Magnetic field coupling among a group of wires can be described with self-impedance of individual wires and mutual-impedance among them. It is assumed in the following sections that these wires are made of linear materials. That assumption is verified through the measurement in Section 4.

2.1 Internal Impedance of Steel Wires

Self-impedance of a wire equals to summation of external inductance and internal impedance [30]. The internal impedance of a wire can be analyzed according the current distribution on the cross section. Therefore, we use a 2D PEEC formulation to obtain the internal impedance of steel wires. The PEEC formulation is derived from the electric field integral equation (EFIE). The current density at a point is expressed by the magnetic vector and electric scalar potentials.

The vector potential $\boldsymbol{A}$ for a linear magnetic material has been well addressed [20, 29], and is given as

$$\boldsymbol{A}(\mathbf{r}) = \boldsymbol{A}_m(\boldsymbol{r}) + \boldsymbol{A}_c(\boldsymbol{r}) \tag{1}$$

where component $\boldsymbol{A_m}(\boldsymbol{r})$ and $\boldsymbol{A_c}(\boldsymbol{r})$ are contributed by magnetic polarization and conductive current respectively. They are given in 2D as

$$\boldsymbol{A}_m(\boldsymbol{r}) = \frac{\mu_0}{2\pi}\int_{S'} \boldsymbol{M}(\boldsymbol{r}') \times \nabla' \left(\frac{1}{\boldsymbol{r} - \boldsymbol{r}'} \right) dS' \tag{2}$$

$$\boldsymbol{A}_c(\boldsymbol{r}) = \frac{\mu_0}{2\pi}\int_{S'} \ln \frac{1}{|\boldsymbol{r} - \boldsymbol{r}'|} \boldsymbol{J}_c(\boldsymbol{r}') dS' \tag{3}$$

where $\boldsymbol{J}$ is the current density and $\boldsymbol{M}$ is the magnetization density. Additional equations need to be built up to solve for unknowns $\boldsymbol{M}$. According to the constitutive relation, the following equation is obtained

$$\boldsymbol{B}(\boldsymbol{r}) = \nabla \times \boldsymbol{A}(\boldsymbol{r}) = \frac{\mu_0 \mu_r}{\mu_r - 1} \boldsymbol{M}(\boldsymbol{r}) \tag{4}$$

where μ_r is the relative permeability of the wire. Equations for two orthogonal components of magnetization density $\boldsymbol{M_x}$ and $\boldsymbol{M_y}$ are established, and expressed at angular frequency ω in the matrix form, as follows

$$\begin{bmatrix} \boldsymbol{Z_c} & \boldsymbol{j\omega Q_x} & \boldsymbol{j\omega Q_y} \\ \boldsymbol{B_{cx}} & \boldsymbol{P_{xx}} & \boldsymbol{P_{xy}} \\ \boldsymbol{B_{cy}} & \boldsymbol{P_{yx}} & \boldsymbol{P_{yy}} \end{bmatrix} \begin{bmatrix} \boldsymbol{I_z} \\ \boldsymbol{M_x} \\ \boldsymbol{M_y} \end{bmatrix} = \begin{bmatrix} \boldsymbol{V_S} \\ \boldsymbol{B_{sx}} \\ \boldsymbol{B_{sy}} \end{bmatrix} \tag{5}$$

where $\boldsymbol{Z_c}$, $\boldsymbol{Q_x}$, $\boldsymbol{Q_y}$, $\boldsymbol{B_{cx}}$, $\boldsymbol{B_{cy}}$, $\boldsymbol{P_{xx}}$, $\boldsymbol{P_{yy}}$, $\boldsymbol{P_{xy}}$ and $\boldsymbol{P_{yx}}$ are square matrices. $\boldsymbol{Z_c}$ is the term associated with the conductive current. Other terms represent couplings between current density and magnetization density. Detail of each term in matrices is presented in Appendix A. In (5) $\boldsymbol{V_s}$ is the external voltage sources, and both $\boldsymbol{B_{sx}}$ and $\boldsymbol{B_{sy}}$ are respectively external magnetic fields in *x* and *y* directions.

Since unknowns $\boldsymbol{M_x}$ and $\boldsymbol{M_y}$ are introduced, matrix relation (5) cannot be directly solved in the traditional circuit solvers, such as PSpice and EMTP. It is preferred to transform the magnetic effect of a wire into current–related components, so that the impedance can be used directly in a circuit solver. By performing elementary operations, (5) reduces to a tradition circuit formulation as

$$[\boldsymbol{Z_{eqv}}] \cdot [\boldsymbol{I_z}] = [\boldsymbol{V_s}] \tag{6}$$

where $\boldsymbol{Z_{eqv}}$ is the obtained equivalent impedance for a linear magnetic wire, and is given as,

$$\begin{aligned} \boldsymbol{Z_{eqv}} = \boldsymbol{Z_c} &+ \boldsymbol{j\omega Q_x} \left(\boldsymbol{P_{xy}} \boldsymbol{P_{yy}^{-1}} \boldsymbol{P_{xy}} - \boldsymbol{P_{xx}} \right)^{-1} \left(\boldsymbol{B_{cx}} - \boldsymbol{P_{xy}} \boldsymbol{P_{yy}^{-1}} \boldsymbol{B_{cy}} \right) \\ &+ \boldsymbol{j\omega Q_y} \left(\boldsymbol{P_{xy}} \boldsymbol{P_{xx}^{-1}} \boldsymbol{P_{xy}} - \boldsymbol{P_{yy}} \right)^{-1} \left(\boldsymbol{B_{cy}} - \boldsymbol{P_{xy}} \boldsymbol{P_{xx}^{-1}} \boldsymbol{B_{cx}} \right) \end{aligned} \tag{7}$$

While, obtained equivalent impedance is the 2D total impedance for the steel wire. Internal impedance equals to total impedance minus external impedance. It is known that the current tends to flow on the conductor surface when the frequency increases. Thus, external impedance can be approximated by the equivalent impedance at high frequency. The internal impedance of the steel wire then is given as,

$$Z_{2D,in}(\omega) = Z_{eqv}(\omega) - j\omega Z_{eqv}(\infty) \tag{8}$$

where $Z_{eqv}(\infty)$ represents the equivalent impedance at infinite high frequency. It was calculated at 10 MHz in building the circuit model of steel wires.

2.2 Self-Impedance of Steel Wires

The external inductance is not affected by the material of the conductor. Since the current tends to flow on the conductor surface at high frequency, internal inductance drops to zero as the frequency increases. External inductance can then be calculated with the formulas for sheets carrying surface current only, as shown in Appendix B. Then, total self-impedance $\boldsymbol{Z_s}$ of a wire equals

$$Z_s(\omega) = Z_{2D,in}(\omega) \cdot l + j\omega L_{3D,ext} \tag{9}$$

where l is the length of the wire, and $L_{3D,ext}$ is the 3D external inductance of the wire calculated using the surface current, The linear magnetic wire can then be simulated in the traditional circuit solver using a traditional impedance model.

2.3 Mutual Inductance among Steel Wires

Mutual coupling between two wires is determined by flux linkage between these wires associated with the currents carried by these wires. The flux linkage of the wires is generally not affected by wire material [31]. Therefore, mutual inductance among steel wires depends on the relative position and lengths of the wires. With filament approximation, it is expressed analytically [32, 33] as

$$L_M = \frac{\mu_0 l}{4\pi} \left[\ln \left(\frac{l}{d} + \sqrt{1 + \frac{l^2}{d^2}} \right) - \sqrt{1 + \frac{d^2}{l^2}} + \frac{d}{l} \right] \tag{10}$$

for aligned conductors of spacing *d*.

2.4 Extended Equivalent Circuit Model

Self-impedance of a wire obtained in (9) are generally frequency-dependent. A time-domain circuit solver cannot be applied directly to the network with such frequency-dependent circuit parameters. A Vector Fitting (VF) method [25] then is adapted to generate the rational approximation of frequency-dependent circuit parameters. Note that mutual inductance varies little with the frequency. This technique is applied to self-impedance of wires only.

Assume that the impedance at the frequencies of interest is available. This impedance can be approximated by rational functions in the form of pole-residue terms as follows:

$$Z(s) = R_0 + sL_0 + \sum_{m=1}^{N} \frac{1}{s - p_m} R_m \tag{11}$$

where terms R_0 and L_0 are constant, and R_m and p_m are the mth residue and pole which are extracted by the VF method. (11) can be transformed into a SPICE compatible form as shown below [34]

$$Z(s) = R'_0 + sL'_0 + \sum_{m=1}^{N} \frac{s}{s - p_m} R'_m \tag{12}$$

where $R'_0 = R_0 - \sum_{m=1}^{N} \frac{1}{p_m} R_m$, $R'_0 = \frac{1}{p_m} R_m$, $L'_m = -\frac{1}{p_m} R'_m$.

A simplified form of the vector fitting equivalent circuit as shown Fig. 1 is adopted in the calculation. The extended equivalent network with frequency-independent parameters can then be established for time-domain simulations.

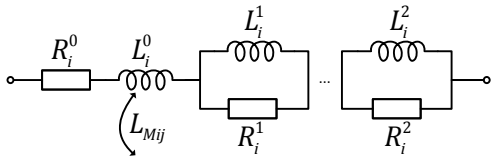

Fig. 1. *Circuit representation of the rational function*

3. Responses of Structural Steels under Large Impulse Current

Unlike electrical steels used as the cores in transformers and motors, structural steels are exposed to lightning and carry the lightning current directly. A large current will flow in the axial direction of the steels. A current injection method was employed to disclose the response of the steels carrying a surge current. As it would be difficult to measure the voltage across a straight wire, a square wire loop was constructed in the laboratory. This loop was connected to an impulse current generator (ICG).

Fig. 2 shows the test setup for surge measurement in a steel wire loop. There are two low-carbon steel samples selected for the experiment; (a) steel bars (Structural Steel Q345) used in telecommunication towers and (b) reinforcing steel rods used in concrete buildings. The side lengths of the steel-bar and steel-rod loops are respectively 1.65m and 1.0m. Other information of these steel wires is given in Table 1.

Table 1 Material and geometric information of steel wires

Material	R_{dc} (mΩ/m)	μ_r	Width (mm)	Thick (mm)
Steel bar	1.28	40	40	4
			Outer Radius (mm)	Inner Radius (mm)
Steel rod	3.16	35	5	0

In the experiment, an impulse current of 10/30 μs with the amplitude from 15 A to 335 A was injected into the loop. Both current and voltage on the loop were measured with digital oscilloscope TDS3022C, as shown in Fig. 2. The recorded time-domain voltage and current were converted into the frequency-domain results using a fast Fourier transform technique. Frequency-domain impedance then was calculated by dividing the voltage by the current. As both current and voltage were weak and noisy at the low and high frequencies, the results in the frequency range from 1 kHz to 50 kHz were extracted for analysis. Note that the primary frequency of the 1st stroke lightning current is in this frequency range.

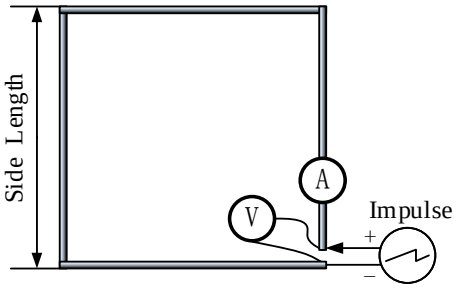

Fig. 2. *Experiment configuration of a steel wire loop*

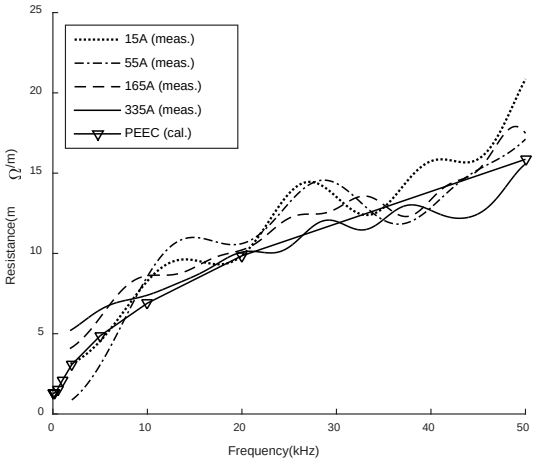

(a)

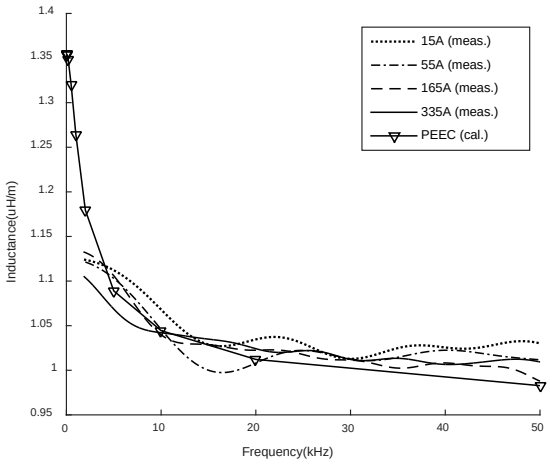

(b)

Fig. 3. *Measured and calculated circuit parameters of a steel bar*

(a) Resistance, ***(b)*** Inductance

Fig. 3 shows both resistance and inductance of the steel bar loop under the impulse current with four different magnitudes. The resistance curves associated with these amplitudes generally match each other, although there are

some fluctuations observed in the figure. These fluctuations generally were caused by noises in the current and voltage measurements. Similar results are observed as well from the inductance curves. This indicates that the steel bar is not sensitive to the current amplitude when it carries the lightning current directly.

The resistance and inductance of the steel bar loop were also calculated with the PEEC approach using the internal impedance of individual wires and partial inductance among wires presented in Section II. In the calculation, the steel bar was represented by a linear magnetic bar with the material and geometric data given in Table 1. The results are plotted in the figure as well. It is clearly seen in the figure that both calculated and measured results match well. As a result, the steel can be represented by a linear magnetic material.

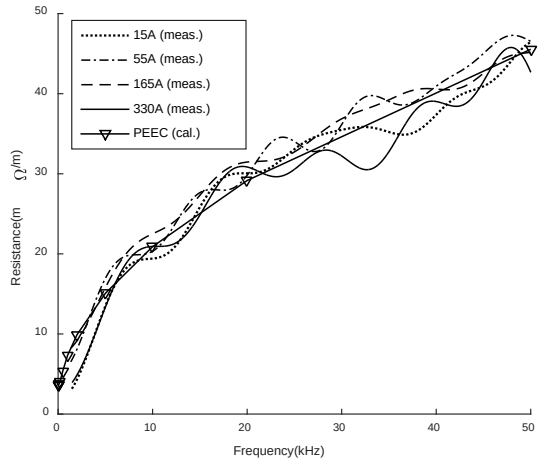

(a)

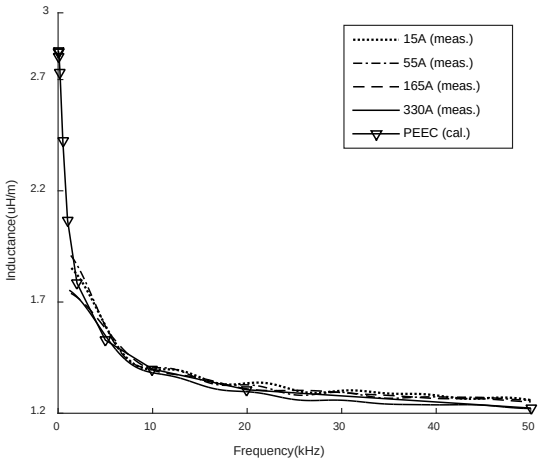

(b)

Fig. 4. *Measured and calculated circuit parameters of a steel rod*
(a) Resistance**, *(b)*** Inductance

A similar measurement was performed for the steel-rod loop. The measured resistance and inductance together with calculated results are presented in Fig. 4. Consistent results are observed. In this case, the steel rod was modelled by a linear magnetic material with the relative permeability of 40. Clearly, both structural steels exhibit weak ferromagnetism, and can be viewed as the linear magnetic material whey they carry a lightning current directly. The circuit parameters of structural steels can then be calculated using linear magnetic formulation as presented in Section II.

As shown in these figures, both resistance and inductance vary significantly with frequency. The resistance of these steel wires increases with increasing frequency due to the skin effect. The resistance of both the steel bar or rod at 50 kHz is approximately ten times as much as its DC resistance. While the inductance of these steel wires decreases with increasing frequency, and tends to be constant at high frequency. This change is due to the decrease of internal inductance arising from the skin effect. At high frequency, the current in a steel wire tends to flow along its surface, and the internal inductance becomes zero.

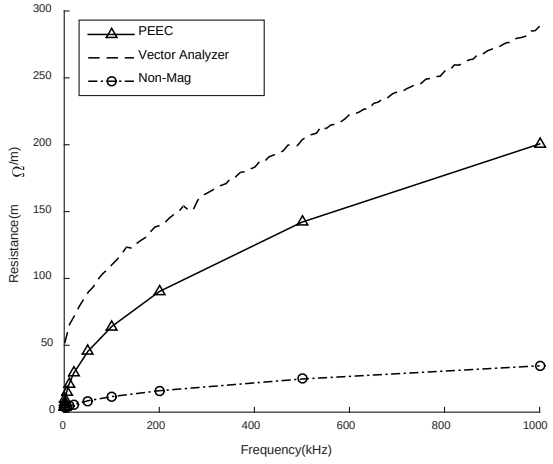

(a)

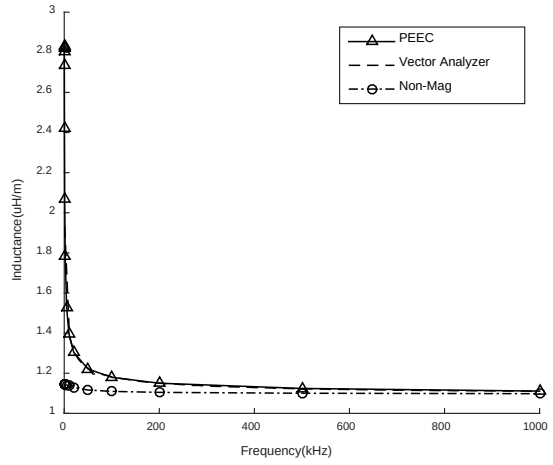

(b)

Fig. 5. *Comparison of resistance and inductance obtained from a vector network analyzer and measured on a steel-rod loop*
(a) Resistance**, *(b)*** Inductance

4. Responses of Structural Steels under Small Current

As one kind of ferromagnetic materials, structural steels may exhibit nonlinear characteristics under certain conditions. To investigate the behavior of structural steels under the excitation of small current, impedance measurement

using a vector network analyzer (Bode 100 VNA) was made on the steel rod presented in Section III. Both equivalent resistance and inductance at individual frequencies were obtained by running a frequency sweep from 1 kHz to 1 MHz with the current magnitude of up to 10 mA. The results are presented in Fig. 5, together with calculated resistance and inductance given in Fig. 4 and the purely-conductive loop (μ_r=1).

To exploit the nonlinear property of the steel rod, the relative permeability of the steel rod under the mA current from the VNA was investigated with the procedure given in Section II. Assume that the steel is replaced with a linear material. Its equivalent relative permeability is determined in such a way that the calculated resistance of this linear steel matches the VNA results at selected individual frequencies. The results are presented in Table 2.

Table 2 Relative permeability of the steel rod carrying small current

Frequency (kHz)	10	50	100	500	1000
μ_r	340	140	106	72	72

It is found that the equivalent relative permeability is equal to 340 at 10 kHz and 106 at 100 kHz. These figures are much greater than the relative permeability at the large impulse current, which does not vary generally with the amplitude of the impulse current. This clearly indicates that the steel sample is nonlinear under the excitation of small current. It is deeply saturated under the lightning current, and can be viewed as a linear magnetic material with low relative permeability

It is also found that the relative permeability is frequency-variant, and decreases with increasing frequency generally. This is consistent with the characteristic of ferromagnetic materials. In this case, it is impossible to obtain a single value of relative permeability suitable for a range of frequencies. Therefore, frequency-dependence and material nonlinearity should be considered when the steel carries a small current.

5. Lightning Current Sharing Experiment

In radio base stations, signal and power cables run on the towers from the top end to the equipment on the ground. As the towers are subject to lightning strikes, lightning current sharing among the structural steel and the cables is one important issue addressed in lightning protection for sensitive equipment on the ground. A laboratory test was conducted to validate the model of the structural steel for lightning current sharing analysis. As it was impossible to generate a lightning return current without a returning path, a wire loop system made of a steel bar and a shielded DC power cable (SDC) was selected for testing, as shown in Fig. 6. In Fig. 6 the SDC cable runs in parallel with the steel bar to form a rectangular loop with the length of 8.3 m and the width of 1.65 m. It consists of two separate core conductors enclosed by the cylindrical sheath, all of which are made of copper. The detailed information of the steel bar and the cable is given in Table 3.

In the experiment, both cable cores and cable sheath were connected to the steel bar at two ends of the loop. An 8/20 μs impulse current with the amplitude of 1 kA and 1.8 kA was injected at one end of the wire system. Currents in both the core and the steel bar were measured and recorded with digital oscilloscope TDS3022C. Simulation of the surge currents in the tested system was also performed in TEAS [5] with the steel model proposed in the previous sections. Perfect ground is used in the calculation.

Table 3 Material and geometric information of conductors

Type		Rdc (mΩ/m)	μ_r	Width (mm)	Thickness (mm)
Steel Bar		1.28	40	40	4
				Outer Radius (mm)	Inner Radius (mm)
SDC Cable	Sheath	14.85	1	4.4	3.9
	Core	5.28	1	1.0	-

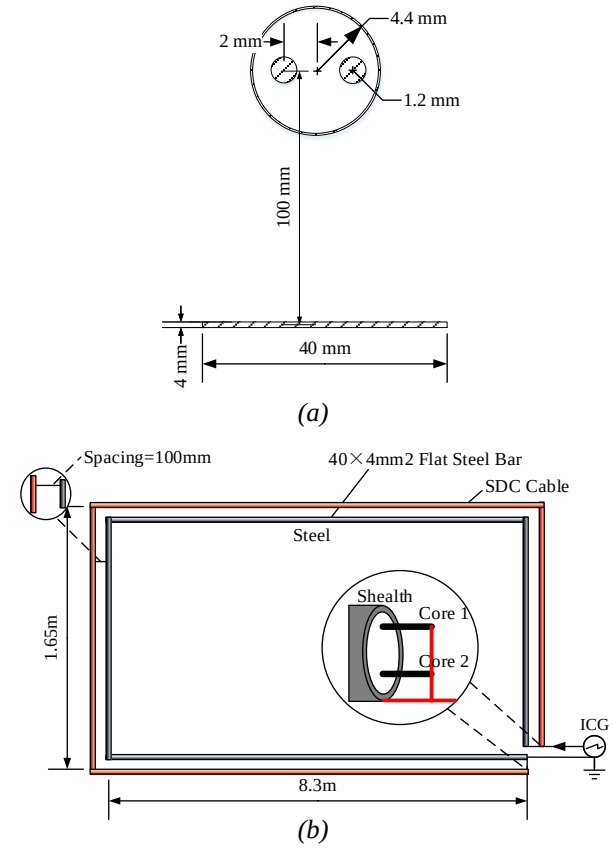

Fig. 6. *Configuration of a cable-steel system under test*

(a) Cross-section view of the setup, ***(b)*** Plan view of the setup

Fig. 7 shows the waveforms of the currents in the steel bar and one of SDC cores, together with the total current injected into the system. These current waveforms were obtained by the laboratory experiment as well as the computer simulation. It is clearly seen that both calculated and measured current waveforms match well in the waveform. Table 4 shows both measured and calculated peak currents in the steel bar and cable core. It is found that good agreements are achieved with the peak-current error of less than 2.5 %. This indicates that the model of the structural steel is reasonably accurate, and is applicable to the analysis of lightning current sharing in the steel wire/copper cable system. It is shown from the figure that the core carries the

current with a relatively long rising time and a low peak value because of the frequency-dependent skin effect.

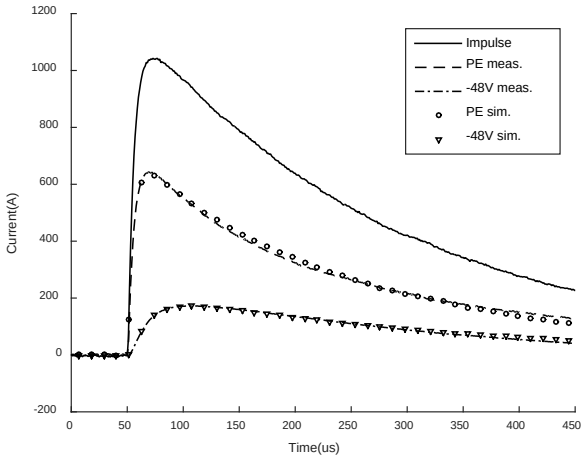

Fig. 7. *Comparison of current waveforms under the 1 kA surge current*

Table 4 Comparison of measured and simulated Peak Currents (unit: A)

Source	Steel			Core of SDC		
	Meas.	Cal.	Err.	Meas.	Cal.	Err.
1.0 kA	640	633	1.1%	172	176	2.3%
1.8 kA	1094	1072	2.0%	285	291	2.1%

6. Conclusion

This paper has presented an investigation into equivalent circuit models of structural steels used in the lightning current analysis. These steels are commonly used in grounded structures, such as building, tower and others. Formulas for calculating circuit parameters of the steel wires were presented. The results of laboratory experiments were included to reveal the surge current response of both steel bars and steel rods. The proposed modelling procedure was applied to analyse lightning current sharing in a steel wire/copper cable system. Good agreements with the experimental results were observed.

It is concluded that these steel wires are deeply saturated when they carry lightning current directly. They can be treated as linear magnetic materials with the relative permeability of 35-40. Such wires are represented by internal impedance and mutual inductance, which can be calculated with an equivalent circuit approach for wires with arbitrary cross sections. With a vector fitting technique, steel wires can be represented with frequency-independent equivalent circuits. Surge current analysis can then be made in the time domain. The equivalent circuit model is primarily for cases with the primary frequency below 50 kHz, but could be extended to higher-frequency applications.

7. Acknowledgments

The work leading to this paper was supported by grants from the Research Committee of the Hong Kong Polytechnic University, and the Research Grants Council of the HKSAR (Project No. 15203815 and 514813).

8. References

[1] V. A. Rakov *et al.*, "Direct lightning strikes to the lightning protective system of a residential building: triggered-lightning experiments," *IEEE Transactions on Power Delivery*, vol. 17, no. 2, pp. 575-586, 2002.

[2] Y. Du and M. L. Chen, "Influence of Building Structures on the Lightning Return Stroke Current," *IEEE Transactions on Power Delivery*, vol. 25, no. 1, pp. 307-315, 2010.

[3] Z. Tong, Z. Dong, and T. Ashton, "Analysis of electric field influence on buildings under high-voltage transmission lines," *IET Science, Measurement & Technology*, vol. 10, no. 4, pp. 253-258, 2016.

[4] N. Rameli, M. Z. A. Ab-Kadir, M. Izadi, C. Gomes, and N. Azis, "Effect of the grounding system on the lightning current profile along a tall structure," *IET Science Measurement & Technology*, vol. 9, no. 6, pp. 717-727, Sep 2015.

[5] H. Chen, Z. Qin, Y. Du, Q. Wang, and Y. Ding, "TAES: A PEEC-based tool for transient simulation," in *2016 Asia-Pacific International Symposium on Electromagnetic Compatibility (APEMC)*, 2016, vol. 1, pp. 676-678: IEEE.

[6] U. Kumar, V. Hegde, and P. B. Darji, "Investigations on voltages and currents in the lightning protection system of the Indian satellite launch pad-I during a stroke interception," *IET Science, Measurement & Technology*, vol. 1, no. 5, pp. 225-231, 2007.

[7] A. Tatematsu, K. Yamazaki, and H. Matsumoto, "Lightning surge analysis of a microwave relay station using the FDTD method," *IEEE Transactions on Electromagnetic Compatibility*, vol. 57, no. 6, pp. 1616-1626, Dec 2015.

[8] A. Rezaei-Zare, M. Sanaye-Pasand, H. Mohseni, S. Farhangi, and R. Iravani, "Analysis of Ferroresonance Modes in Power Transformers Using Preisach-Type Hysteretic Magnetizing Inductance," *IEEE Transactions on Power Delivery*, vol. 22, no. 2, pp. 919-929, 2007.

[9] F. C. F. Guerra and W. S. Mota, "Magnetic core model," *IET Science, Measurement & Technology*, vol. 1, no. 3, pp. 145-151, 2007.

[10] A. E. Ruehli, "Inductance Calculations in a Complex Integrated-Circuit Environment," *IBM Journal of Research and Development*, vol. 16, no. 5, pp. 470-&, 1972.

[11] A. Ruehli, C. R. Paul, and J. Garrett, "Inductance calculations using partial inductances and macromodels," in *IEEE International Symposium on Electromagnetic Compatibility*, 1995, pp. 23-28: IEEE.

[12] K. M. Coperich, A. E. Ruehli, and A. Cangellaris, "Enhanced skin effect for partial-element equivalent-circuit (PEEC) models," *IEEE Transactions on Microwave Theory and Techniques*, vol. 48, no. 9, pp. 1435-1442, 2000.

[13] A. Rong and A. C. Cangellaris, "Generalized PEEC models for three-dimensional interconnect structures and integrated passives of arbitrary shapes," in *Electrical Performance of Electronic Packaging, 2001*, 2001, pp. 225-228: IEEE.

[14] A. E. Ruehli, G. Antonini, J. Esch, J. Ekman, A. Mayo, and A. Orlandi, "Nonorthogonal PEEC formulation for time- and frequency-domain EM and circuit modeling," *IEEE Transactions on Electromagnetic Compatibility*, vol. 45, no. 2, pp. 167-176, 2003.

[15] D. Gope, A. Ruehli, and V. Jandhyala, "Solving Low-Frequency EM-CKT Problems Using the PEEC Method," *IEEE Transactions on Advanced Packaging*, vol. 30, no. 2, pp. 313-320, 2007.

[16] T. Le-Duc, O. Chadebec, J. M. Guichon, and G. Meunier, "Coupling between partial element equivalent circuit method and an integro-differential approach for solving electromagnetics problems," *IET Science Measurement & Technology*, vol. 6, no. 5, pp. 394-397, Sep 2012.

[17] H. Chen, Y. Du, and M. Chen, "Lightning current among closely-spaced cables," in *2014 International Conference on Lightning Protection (ICLP)*, 2014, pp. 412-417.

[18] S. Z. Mei and Y. I. Ismail, "Modeling skin and proximity effects with reduced realizable RL circuits," *IEEE Transactions on Very Large Scale Integration (Vlsi) Systems*, vol. 12, no. 4, pp. 437-447, Apr 2004.

[19] Y. Du, H. Chen, and M. Chen, "Analysis of Transient Magnetic Shielding Made by Conductive Plates With a PEEC Method," *IEEE Transactions on Magnetics*, vol. 53, no. 6, pp. 1-4, 2017.

[20] G. Antonini, M. Sabatini, and G. Miscione, "PEEC modeling of linear magnetic materials," in *2006 IEEE International Symposium on Electromagnetic Compatibility*, 2006, vol. 1, pp. 93-98.

[21] N. H. Xia and Y. Du, "An Efficient Modeling Method for 3-D Magnetic Plates in Magnetic Shielding," *IEEE Transactions on Electromagnetic Compatibility*, vol. 56, no. 3, pp. 608-614, Jun 2014.
[22] D. Romano and G. Antonini, "Quasi-Static Partial Element Equivalent Circuit Models of Linear Magnetic Materials," *IEEE Transactions on Magnetics*, vol. 51, no. 7, pp. 1-15, 2015.
[23] D. Romano and G. Antonini, "Augmented Quasi-Static Partial Element Equivalent Circuit Models for Transient Analysis of Lossy and Dispersive Magnetic Materials," *IEEE Transactions on Magnetics*, vol. 52, no. 5, pp. 1-11, 2016.
[24] Y. Hackl, P. Scholz, W. Ackermann, and T. Weiland, "Efficient Simulation of Magnetic Components Using the MagPEEC-Method," *IEEE Transactions on Magnetics*, vol. 53, no. 3, pp. 1-9, 2017.
[25] B. Gustavsen and A. Semlyen, "Rational approximation of frequency domain responses by vector fitting," *IEEE Transactions on Power Delivery*, vol. 14, no. 3, pp. 1052-1061, Jul 1999.
[26] G. Antonini, D. Deschrijver, and T. Dhaene, "A comparative study of vector fitting and orthonormal vector fitting techniques for EMC applications," in *Electromagnetic Compatibility, 2006. EMC 2006. 2006 IEEE International Symposium on*, 2006, vol. 1, pp. 6-11: IEEE.
[27] D. Deschrijver, M. Mrozowski, T. Dhaene, and D. De Zutter, "Macromodeling of multiport systems using a fast implementation of the vector fitting method," *IEEE Microwave and Wireless Components Letters*, vol. 18, no. 6, pp. 383-385, Jun 2008.
[28] *IEC Standard 62305-1*, 2010.
[29] N. Xia, "PEEC method for evaluating magnetic shielding by metal structures at low frequency," The Hong Kong Polytechnic University, 2013.
[30] F. Dawalibi, "Electromagnetic fields generated by overhead and buried short conductors part 2-ground networks," *IEEE Transactions on Power Delivery*, vol. 1, no. 4, pp. 112-119, 1986.
[31] N. R. Center, "Circular Magnetic Fields Distribution and Intensity," *https://www.nde-ed.org/EducationResources/CommunityCollege/MagParticle/Physics/CircularFields.htm*.
[32] F. W. Grover, *Inductance calculations: working formulas and tables.* Dover, 1946.
[33] C. R. Paul, *Inductance: Loop and Partial*. Wiley, 2011.
[34] K. M. Coperich, J. Morsey, V. I. Okhmatovski, A. C. Cangellaris, and D. E. Ruehli, "Systematic development of transmission-line models for interconnects with frequency-dependent losses," *IEEE Transactions on Microwave Theory and Techniques*, vol. 49, no. 10, pp. 1677-1685, Oct 2001.
[35] C. Hoer and C. Love, "Exact Inductance Equations for Rectangular Conductors with Applications to More Complicated Geometries," (in English), *Journal of Research of the National Bureau of Standards Section C-Engineering and Instrumentation*, vol. C 69, no. 2, pp. 127-+, 1965.

Appendix A

To consider the skin, proximity and magnetic effect, the cross section of the conductor is discretized into small rectangular cells. Fig. A1 illustrates the typical discretization for rectangle and irregular cross sections. Both current density J_{ci} and magnetization densities M_{xi} and M_{yi} in cell i are assumed constant. Voltage V_i in cell i is contributed by the resistive voltage of the cell itself, and inductive voltage coupled to all cells. It is given as

$$V_i = \frac{J_{ci}}{\sigma} + j\omega\frac{\mu_0}{2\pi}\sum_{i=1}^{N}\int_{S_i}\ln\frac{1}{|\Delta r|}J_{ci}dS + j\omega\frac{\mu_0}{2\pi}\sum_{i=1}^{N}\int_{S_i}\left(\frac{u}{\Delta r^2}M_{xi}-\frac{v}{\Delta r^2}M_{yi}\right)dS \tag{A1}$$

where N is the number of discretization cells, and $u=x-x'$u = x-x', $v=y-y'$ and $\Delta r=r-r'$.

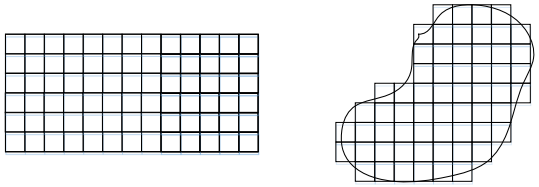

Fig. A1. *Discretization of the cross section of wires.*

Taking advantage of the constitutive relation, equations for two orthogonal components of magnetization density M_{xi} and M_{yi} are established, as follows

$$0 = \frac{\mu_0}{2\pi}\sum_{i=1}^{N}\int_{S_i}\ln\frac{-v}{\Delta r^2}J_{ci}dS + \frac{\mu_0}{2\pi}\sum_{i=1}^{N}\int_{S_i}\frac{u^2-v^2}{\Delta r^4}M_{xi}dS + \frac{\mu_0}{2\pi}\sum_{i=1}^{N}\int_{S_i}\frac{2uv}{\Delta r^4}M_{yi}dS - \frac{\mu_0\mu_r}{\mu_r-1}M_{xi} \tag{A2}$$

$$0 = \frac{\mu_0}{2\pi}\sum_{i=1}^{N}\int_{S_i}\ln\frac{u}{\Delta r^2}J_{ci}dS + \frac{\mu_0}{2\pi}\sum_{i=1}^{N}\int_{S_i}\frac{2uv}{\Delta r^4}M_{xi}dS + \frac{\mu_0}{2\pi}\sum_{i=1}^{N}\int_{S_i}\frac{v^2-u^2}{\Delta r^4}M_{yi}dS - \frac{\mu_0\mu_r}{\mu_r-1}M_{yi} \tag{A3}$$

The system of linear equations is now established, and can be expressed in the matrix form as shown in (5), where detail of each term in matrices is computed using point-matching method as below

$$\begin{aligned}
\boldsymbol{Z_c} &= \sum_{i=1}^{N}\frac{1}{\sigma dS_i} + j\omega\frac{\mu_0}{2\pi}\sum_{i=1}^{N}\int_{S_i}\ln\frac{1}{|\Delta r|}dS \\
\boldsymbol{Q_x} &= \frac{\mu_0}{2\pi}\sum_{i=1}^{N}\int_{S_i}\frac{v}{\Delta r^2}dS \\
\boldsymbol{Q_y} &= \frac{\mu_0}{2\pi}\sum_{i=1}^{N}\int_{S_i}\frac{-u}{\Delta r^2}dS \\
\boldsymbol{P_{xx}} &= \frac{\mu_0}{2\pi}\sum_{i=1}^{N}\int_{S_i}\left(\frac{4u^2}{\Delta r^4}-\frac{2}{\Delta r^2}\right)dS - \frac{\mu_0}{\mu_r-1} \\
\boldsymbol{P_{yy}} &= \frac{\mu_0}{2\pi}\sum_{i=1}^{N}\int_{S_i}\left(\frac{4v^2}{\Delta r^4}-\frac{2}{\Delta r^2}\right)dS - \frac{\mu_0}{\mu_r-1} \\
\boldsymbol{P_{xy}} &= \frac{\mu_0}{2\pi}\sum_{i=1}^{N}\int_{S_i}\frac{2uv}{\Delta r^2}dS \\
\boldsymbol{B_{cx}} &= -\boldsymbol{Q_x} \quad \boldsymbol{B_{cy}} = -\boldsymbol{Q_y} \quad \boldsymbol{P_{xy}} = \boldsymbol{P_{yx}}
\end{aligned} \tag{A4}$$

Appendix B

The external inductance of a conductor is determined by the associated magnetic vector potential outside the conductor. It can be therefore calculated using the concept of surface current on the conductor. For a conductor with the irregular cross section, its outer surface can be approximated with a set of planes or sheets which run either in parallel or perpendicularly. The external inductance of such a conductor can then be expressed by using self- and mutual inductance of these sheets.

Without loss of generality, a rectangular conductor as shown in Fig. B1 is selected to illustrate the procedure of external inductance calculation. Assume that L_a and L_b are the self-inductance of Sheets A_1 and B_1, M_a and M_b are mutual inductance between two parallel sheets, and M_{ab} is mutual

inductance of two perpendicular sheets. By neglecting resistive voltage drop, voltages along these four sheets are expressed as

$$\begin{bmatrix} V_{a1} \\ V_{b1} \\ V_{a2} \\ V_{b2} \end{bmatrix} = j\omega \begin{bmatrix} L_a & M_{ab} & M_{aa} & M_{ab} \\ M_{ab} & L_b & M_{ab} & M_{bb} \\ M_{aa} & M_{ab} & L_a & M_{ab} \\ M_{ab} & M_{bb} & M_{ab} & L_b \end{bmatrix} \cdot \begin{bmatrix} I_{a1} \\ I_{b1} \\ I_{a2} \\ I_{b2} \end{bmatrix} \quad \text{(B1)}$$

or in short form

$$\boldsymbol{V} = j\omega \boldsymbol{L}\boldsymbol{I} \quad \text{(B2)}$$

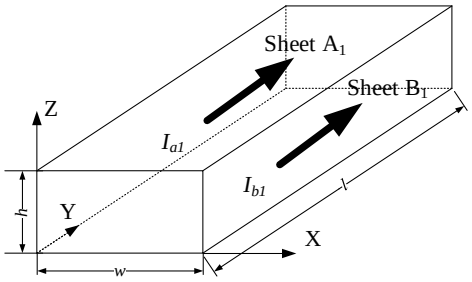

Fig. B1. *Configuration of a rectangular conductor*

Note that voltages on these sheets are same as they are connected in parallel. External inductance of this conductor then is given as

$$L_{ext} = \frac{V_{a1}}{j\omega(I_{a1} + I_{b1} + I_{a2} + I_{b2})} = \frac{1}{\sum_i^4 \sum_j^4 Y_{ij}} \quad \text{(B3)}$$

where Y_{ij} is the ijth elements of the inverse of matrix $\boldsymbol{L}$.

The inductance of sheets or plates with zero thickness has been discussed extensively in [35]. For easy reference, these inductance formulas are presented in the appendix. For two parallel horizontal planes with sheet spacing of Δz, mutual inductance is expressed as

$$M_{=} = \frac{\mu_0}{4\pi} \frac{1}{W_i W_j} \sum_{x_1}^{x_2} \sum_{y_2}^{y_1} \sum_{x_1'}^{x_2'} \sum_{y_1'}^{y_2'} f_1(x - x', y - y', \Delta z) \quad \text{(B4)}$$

where W_i and W_j are the widths of these two sheets. Function $f_1(u,v,w)$ in (B4) is given as

$$f_1(u,v,w) = \frac{v^2 - w^2}{2} u \ln(u + R) + \frac{u^2 - w^2}{2} v \ln(v + R) - \frac{1}{6}(R^2 - 3w^2)R - uvw \tan^{-1}\left(\frac{uv}{wR}\right)$$

and $R = \sqrt{u^2 + v^2 + w^2}$. Self-inductance of a sheet can be calculated with (B4) as well by setting Δz=0. For two perpendicular sheets (e.g., Sheets A_1 and B_1), mutual inductance is expressed as

$$M_{\perp} = \frac{\mu_0}{4\pi} \frac{1}{W_i W_j} \sum_{z_1}^{z_2} \sum_{y_2}^{y_1} \sum_{x_1'}^{x_2'} \sum_{y_1'}^{y_2'} f(w - x', y - y', z - h) \quad \text{(B5)}$$

where function $f_2(u,v,w)$ in (B5) is given as

$$f_2(u,v,w) = \left(\frac{v^2}{2} - \frac{w^2}{6}\right) w \ln(u + R) + \left(\frac{v^2}{2} - \frac{u^2}{6}\right) u \ln(w + R) + uvw \ln(v + R) - \frac{uw}{3} R - \frac{v^3}{6} \tan^{-1}\left(\frac{uw}{vR}\right) - \frac{vu^2}{2} \tan^{-1}\left(\frac{vw}{uR}\right) - \frac{vw^2}{2} \tan^{-1}\left(\frac{vu}{wR}\right)$$